

Materials Advances

Accepted Manuscript

This article can be cited before page numbers have been issued, to do this please use: H. M. Sivaprakasam, R. Parasuraman and A. Anand Prabu, *Mater. Adv.*, 2026, DOI: 10.1039/D6MA00411C.



This is an Accepted Manuscript, which has been through the Royal Society of Chemistry peer review process and has been accepted for publication.

Accepted Manuscripts are published online shortly after acceptance, before technical editing, formatting and proof reading. Using this free service, authors can make their results available to the community, in citable form, before we publish the edited article. We will replace this Accepted Manuscript with the edited and formatted Advance Article as soon as it is available.

You can find more information about Accepted Manuscripts in the [Information for Authors](#).

Please note that technical editing may introduce minor changes to the text and/or graphics, which may alter content. The journal's standard [Terms & Conditions](#) and the [Ethical guidelines](#) still apply. In no event shall the Royal Society of Chemistry be held responsible for any errors or omissions in this Accepted Manuscript or any consequences arising from the use of any information it contains.

Cite this: DOI: 00.0000/xxxxxxxxxx

Low-Temperature Molten Salt Shielded Synthesis of Semiconducting Mn-doped β -FeSi₂ in ambient air condition

Hemalatha M. Sivaprakasam †, Rajasekar Parasuraman†*, Arun Anand Prabu†*

Received Date

Accepted Date

DOI: 00.0000/xxxxxxxxxx

β -FeSi₂ has emerged as a promising, low-cost, and eco-friendly semiconducting material with strong potential for energy-related applications. However, conventional synthesis methods typically require high temperatures and controlled environments such as vacuum or inert atmospheres, which increase manufacturing costs and limit scalability. In this work, we report an economical and scalable molten salt shielded synthesis method for producing semiconducting Mn-doped β -FeSi₂ with minor Si and oxide secondary phases, which was confirmed using X-ray diffraction. Morphology and nominal elemental composition were examined using field-emission scanning electron microscopy and energy-dispersive X-ray spectroscopy. Furthermore, X-ray photoelectron spectroscopy was employed to investigate the surface chemical composition of the synthesized material. Temperature-dependent resistivity measurements of the as-synthesized pellet confirms its semiconducting behavior. Overall, the results demonstrate that the MS3 is a simple, scalable, and cost-effective approach for preparing semiconducting β -FeSi₂ in powder form. The obtained powder can be utilized for fabricating composite or flexible devices for energy-related applications.

1 Introduction

Semiconducting materials synthesized in nano/micro scale powder form can be incorporated into polymer matrices to form functional composite materials. These composite materials are used in fabrication of flexible thermoelectric modules, flexible solar cells and flexible electronics. The powder-polymer approach enables low-temperature processing, mechanical flexibility, and scalable solution-based manufacturing techniques, making it attractive for next-generation wearable and large-area energy devices. Semiconducting transition metal silicides (TMs) show excellent electrical conductivity, stability, and potent resistance to corrosion and oxidation. Among the various transition metal silicides, β -FeSi₂ garnered widespread interest because of its stability in higher temperature and harsh chemical environments. β -FeSi₂ is a semiconducting material with band gap value of 0.8 eV and crystallizes in orthorhombic *Cmca* space group. It consists of the elements which are earth abundant, low cost, non-toxic and environmentally friendly in nature. Intrinsic β -FeSi₂ can be made in to either n-type by doping Co, Ni (Fe site) / P doping (Si site) or p-type by doping it with Mn, Cr (Fe site) / Al (Si site)^{1,2}.

From the literature, Intrinsic β -FeSi₂ show the room temperature resistivity values in the range of 10¹-10³ Ω .cm with the

carrier concentration of $\sim 10^{14}$ - 10^{16} cm⁻³ and mobility values of 10-200 cm².V⁻¹.s⁻¹. This reflects its low intrinsic carrier density and semiconducting nature^{3,4}. Upon n-type β -FeSi₂ doping, the carrier concentration increases significantly to about 10¹⁷-10¹⁸ cm⁻³. The mobility falls in the range of 5-100 cm².V⁻¹.s⁻¹, due to the doping, resistivity decreases in the range of 1-10⁻³ Ω .cm. Similarly, p-type β -FeSi₂ exhibits the resistivity 10-10⁻² Ω .cm with carrier concentrations approximately 10¹⁷-10¹⁹ cm⁻³, and mobilities in the range of 2-50 cm².V⁻¹.s⁻¹, depending on dopant type and concentration⁵⁻⁹. Recent studies have shown that improved thermoelectric performance in β -FeSi₂ achieved through densification, microstructural optimization and doping, which enhance grain connectivity and reduce interfacial resistance¹⁰⁻¹³. The excellent high temperature stability, environmental friendliness and tuneable carrier type and the carrier concentration makes β -FeSi₂ as a potential material for photovoltaic, thermoelectric, and optoelectronic applications.

The Fe-Si binary phase diagram exhibits complex interactions between metallic phases (Fe, α -Fe₂Si₅, and ϵ -FeSi) and semiconducting phases (β -FeSi₂ and Si). β -FeSi₂ does not form directly from the melt. During the initial solidification of arc melted Fe and Si, α -Fe₂Si₅ and ϵ -FeSi are formed, which subsequently heat treated (873-1073 K for 12-100 h) to produce β -FeSi₂. However, this peritectoid reaction between the metallic α and ϵ phases proceeds very slowly and show sluggish kinetics (α -Fe₂Si₅ + ϵ -FeSi \rightarrow β -FeSi₂)^{14,15}. As an alternative approach, arc melting with

Department of Chemistry, School of Advanced Sciences, Vellore Institute of Technology, Vellore, Tamil Nadu, India - 632 014, E-mail: rajasekarmgac@gmail.com; anandprabu@vit.ac.in



excess Si leads to the formation of α -Fe₂Si₅ along with residual silicon. Subsequent heat treatment facilitates the eutectoid reaction below 1138 K (α -Fe₂Si₅ \rightarrow β -FeSi₂ + Si). This eutectoid-based route significantly reduces the reaction time and results in the formation of a Si-dispersed β -FeSi₂ composite^{16–20}.

As another approach, direct solid-state reaction between Fe and Si is carried out by ball milling or reactive sintering below 973 K to achieve the formation of β -FeSi₂. Ur et al. synthesized Co-doped n-type FeSi₂ using mechanical alloying followed by heat treatment at \sim 1073 K, which promotes the formation of β -FeSi₂ with improved electrical transport properties. These studies demonstrate that mechanical alloying enables controlled phase formation and improved microstructural characteristics in FeSi₂-based thermoelectric materials²¹. Yamada et al. reported the low-temperature synthesis of β -FeSi₂ powder using a sodium melt method, where sodium melt was used as the reaction medium and elemental Fe and Si were reacted in a ratio of 1:2.25–2.5 under an argon atmosphere.^{22,23} The reported reaction time ranged from 1.5 to 24 h at temperatures between 673 and 1073 K. This sodium flux method has also been used to synthesize other silicides such as MnSi_{1.7}, CrSi₂, and CoSi. The conventional sodium flux method used for silicide synthesis requires inert or vacuum conditions due to the high reactivity of sodium moisture and oxygen. Although semiconducting β -FeSi₂ can be synthesized by methods such as arc melting, induction melting, ball milling, spark plasma sintering (SPS), hot pressing, mechanical alloying, and chemical synthesis in both bulk and thin-film forms, most of these approaches require an argon atmosphere or vacuum and prolonged heat treatment to stabilize the semiconducting β -FeSi₂. β -FeSi₂ is known as a potential candidate for next-generation low-cost thin-film solar cells and has been widely studied for high-temperature thermoelectric applications^{24–28}.

Despite having the abundant and low-cost constituent elements, the prolonged, multiple processing steps with vacuum requirement involved in synthesizing and stabilizing the phase increases the cost. This makes it important to develop a simple, low-cost method to synthesize β -FeSi₂. Dash et al. introduced Molten Salt Shielded Synthesis (MS³ or MS3) to facilitate the synthesis of MAX phase Ti₃AlC₂, without requiring a vacuum or inert gas atmosphere²⁹. In this method the Molten salt acts as a barrier to prevent oxidation at elevated temperatures. Further in the MXene literature, the synthesis of MAX phase using different molten salts and tuning the properties has been widely studied. In this work, we demonstrate a molten salt shielded synthesis approach for the preparation of Mn-doped β -FeSi₂ powders under ambient air conditions using KBr encapsulation. In this work, KBr encapsulation is employed as a halide-based barrier to limit oxygen interaction during high-temperature processing. This approach suppresses oxidation and enables the synthesis of β -FeSi₂ under ambient conditions without the need for vacuum or inert atmosphere. This strategy provides a simpler and more scalable alternative to conventional molten salt and sodium flux methods. The optimized synthesis protocol to achieve semiconducting Mn-doped β -FeSi₂ with minor Si and oxide secondary phases. This work aims to adopt the molten salt shielded synthesis method to produce oxidation prone semiconducting materials in powder

form under ambient air conditions.

2 Materials and Methods

2.1 Synthesis

Elemental iron (Fe, \geq 99.6%, Sigma Aldrich), silicon (Si, \geq 99.5%, Alfa Aesar, \sim 325 mesh), and potassium bromide (KBr) powders were used as starting materials. Manganese (Mn, \geq 99.6%, Alfa Aesar) was added as a dopant. The nominal composition of the sample was Fe_{1.99}Mn_{0.01}Si₅. The required amounts of the powders were weighed and manually ground for 20 minutes using an agate mortar and pestle. The mixed powder was cold pressed into 10 mm pellets using a hydraulic press at 4 tons for 10 minutes. For encapsulation, a 13 mm die was first partially filled with KBr Powder. The compacted pellet was placed at the center and completely covered with additional KBr to ensure full encapsulation. This assembly was then pressed again at 4 tons for 5 minutes, this process formed a protective KBr layer around the green pellet containing Fe, Si, and Mn. During heat treatment, this KBr layer acts as a physical barrier that limits direct exposure of the pellet to air. The encapsulated pellet was positioned within the center of the salt bed in the alumina crucible and subjected to heat treatment under different temperature–time profiles, and each sample was named using its heat-treatment conditions followed by the prefix “FS”. The sample encapsulated and heat-treated at 1073 K for 24 h was named “FS-1073K/24h”. The sample treated at ‘ for 1 h followed by 1073 K for 4 h was named “FS-1273K/1h-1073K/4h”. The sample treated at 1273 K for 15 minutes and then at 1073 K for 24 h was denoted as FS-1273K/15min-1073K/12h. After heat treatment, the samples were cooled to room temperature and washed with water to completely dissolve the KBr salt, the reacted compacted pellet was filtered. The dissolved salt solution was dried, and the recovered KBr salt was reused. A schematic of the synthesis process is shown in Figure 1.

2.2 Characterization

The crystal structure and phase purity of the samples were examined using X-ray diffraction (XRD, Panalytical X’Pert3) with Cu K α radiation ($\lambda = 1.5406\text{\AA}$). The XRD patterns were analyzed using Rietveld refinement in the GSAS-II software to confirm phase purity and determine the lattice parameters of the prepared samples. The sample morphology was studied using a field-emission scanning electron microscope (FESEM, FEI Quanta 250 FEG). Elemental distribution was analyzed using EDS with an Oxford Instruments detector attached to the FEI Quanta 250 FEG. The density of Mn-doped β -FeSi₂ was measured using Archimedes’ principle. Surface chemical composition and the electronic states of the elements were investigated using X-ray photoelectron spectroscopy (XPS, ULVAC-PHI Versaprobe 4, Japan) equipped with a monochromatic Al K α source. The XPS data were analyzed using XPSPEAK41.

Room-temperature and temperature-dependent electrical resistivity were measured using a home-built four-probe apparatus based on the Van der Pauw method. The room-temperature Seebeck coefficient was measured on the as-synthesized pellet using a home-built setup. In this setup, the sample was placed between



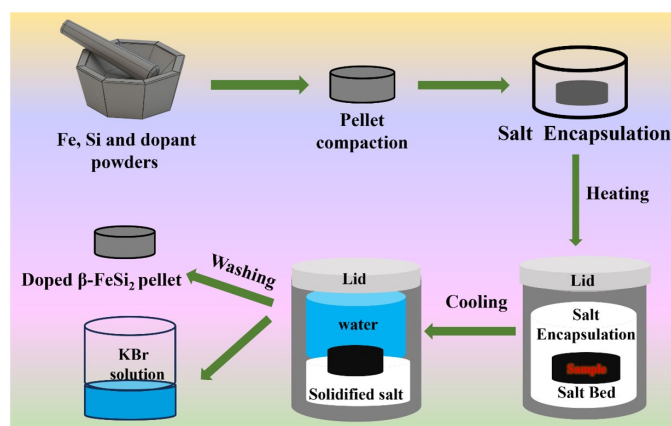


Fig. 1 Schematic of synthesis steps involved in β -FeSi₂ synthesis.

two copper blocks, with one block heated using a micro-heater. The temperature difference between the blocks was monitored using a K-type thermocouple connected in differential mode. The voltage was measured using copper wires soldered onto the blocks, and the Seebeck coefficient was calculated as $\Delta V/\Delta T$, under steady-state conditions.

3 Results and Discussion

Samples synthesized through the molten salt shielded synthesis method with different heating profiles were analyzed using X-ray diffraction, and the data are presented in Figure 2a. The diffraction pattern labeled FS-1073K/24h corresponds to the encapsulated pellet heat treated at 1073 K for 24 h. Detailed phase analysis shows the presence of Si, ϵ -FeSi, and α -Fe₂Si₅, indicating incomplete reaction between the Fe and Si powders. To facilitate the faster eutectoid decomposition reaction to form β -FeSi₂, the encapsulated pellets were initially heat treated at 1273 K for 15 minutes to 1 h. As per the phase diagram and earlier reports¹⁴, this treatment leads to the formation of α -Fe₂Si₅. These pellets were further heat treated at 1073 K for different durations (4, 12, and 24 h). The XRD patterns of the pellets heat treated at 1273 K for 15 minutes followed by 1073 K for 4, 12, and 24 h are shown in Figure 2a. Phase analysis reveals mixed α - and ϵ -phases with minor silicon content for samples heat treated for 4 and 12 h. However, the pellet heat treated at 1273 K for 15 minutes followed by 1073 K for 24 h shows peaks corresponding to β -FeSi₂ and Si only, indicating the formation of β -FeSi₂ with Si as a secondary phase. Rietveld analysis of the diffraction pattern for the sample FS-1273K/15min-1073K/24h was carried out, and the results are shown in Figure 2b. The refinement confirms that the pellet is X-ray pure and the phase fractions along with the calculated lattice parameters are given in Table 1. These results confirm that the two-step heat treatment is essential for achieving the formation of β -FeSi₂ phase.

The refined lattice parameters agree well with the orthorhombic crystal structure of β -FeSi₂, matching the reference pattern (ICSD #9119). Silicon (Si) was detected as a secondary phase, which is expected from eutectoid decomposition. The intentional excess of Si promoted the formation of β -FeSi₂ while suppress-

ing the formation of other iron-rich silicide phases. Figure 3a and b show the secondary electron micrographs of the sample heat treated at 1273 K for 15 minutes followed by 1073 K for 24 h. The microstructure appears rough and porous, consisting of irregularly shaped particles. Some regions display partially sintered material, indicating incomplete densification resulting from the low-temperature eutectoid decomposition treatment. This porous morphology is anticipated to increase interfacial resistance, thereby affecting transport properties. Further, Elemental analysis of the sample surface was performed using energy dispersive spectroscopy (EDS), and the results are shown in Figure 3c-f. The EDS mapping confirms a uniform distribution of Fe and Si, indicating good chemical homogeneity in the synthesized sample. The EDS spectrum shows major peaks for Fe and Si, with a low-intensity peak corresponding to Mn. The elemental mapping (Figure 3d-f) shows the weight percentages of Fe and Si to be 52.9 wt.% and 46.2 wt.%, respectively. Elemental distribution mapping of Mn from EDS exhibits a homogeneous dopant distribution. While EDS mapping confirm the presence and uniform distribution and the absence of any nanoscale secondary phases. Also no secondary Mn containing phases were detected within the detection limit of XRD. Considering low Mn concentration used in this study, which is well within the reported solubility limits in β -FeSi₂. So Mn incorporation into the β -FeSi₂ is possible. X-ray photoelectron spectroscopy (XPS) was performed to understand the chemical environment and oxidation states of the elements present on the sample surface. Figure 4a depicts the XPS survey spectrum of Mn-doped β -FeSi₂, which confirms the presence of elements Fe, Si and Mn. Figure 4b corresponds to Fe 2p, in this peak at 707.5 eV and 720.2 eV have been assigned as spin orbit doublet corresponding to Fe 2p_{3/2} and Fe 2p_{1/2} of Fe-Si bond^{30,31}. The area ratio between the peaks were 2:1 and the splitting energy was 12.7 eV. The peak at 711-713 eV and 723-730 eV of Fe 2p spectrum was deconvoluted to two peaks they are associated to the oxidized Fe and satellite components suggesting possible surface oxide with core silicide. The Si 2p spectrum (Figure 4c) shows a broad peak between 101-103 eV, indicating the presence of Si in SiO₂ indicating the surface oxidation. The peak at 98.8 eV corresponds to the Si present in FeSi₂ lattice and in elemental



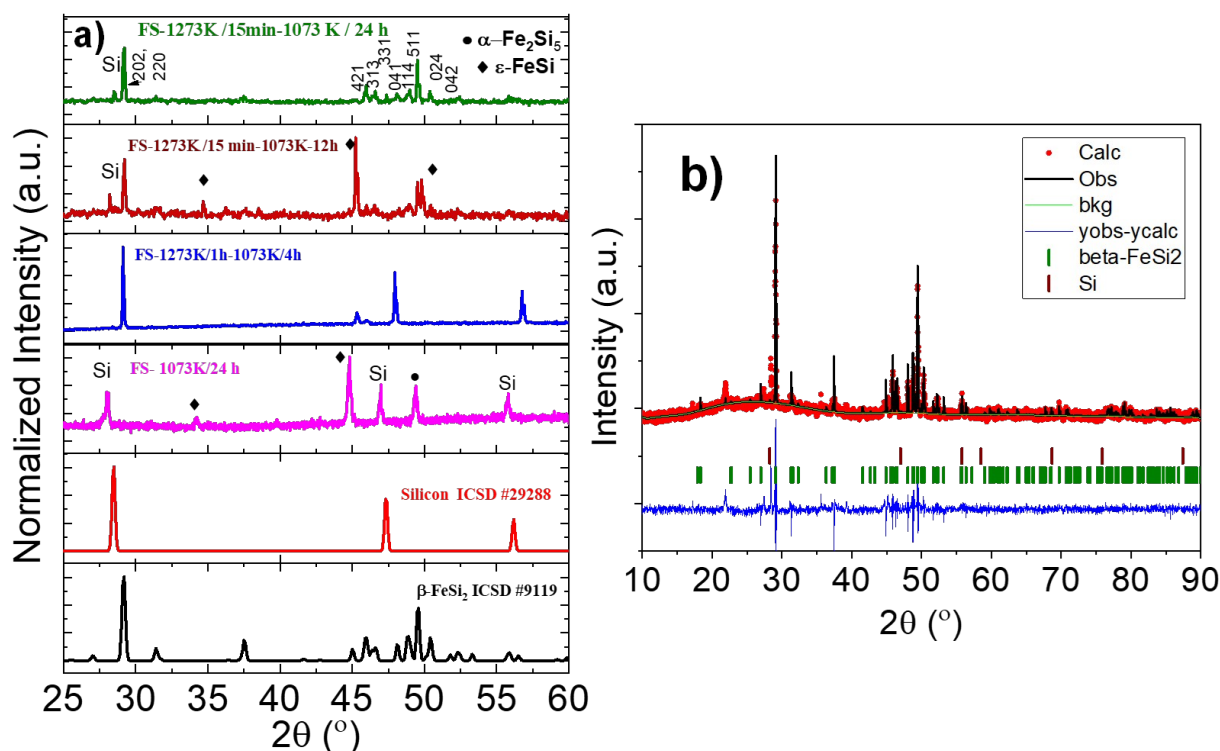


Fig. 2 a) X-ray diffraction pattern of Mn doped β -FeSi₂ samples synthesized using various heat treatment conditions, b) Rietveld Refinement of the sample FS-1273K/15min-1073K/24h.

Table 1 Lattice parameter and phase fractions of the encapsulated pellet FS-1273K/15min-1073K/24h

Sample	Density	Phases present	Wt. %	Lattice Parameter (Å)	GOF	wR
FS-1273/15min-1073K/24h	2.92	β -FeSi ₂ Si	97.5 2.5	a = 9.8763(2), b = 7.7900(5), c = 7.8368 (4) a = 5.4291	1.43	3.16

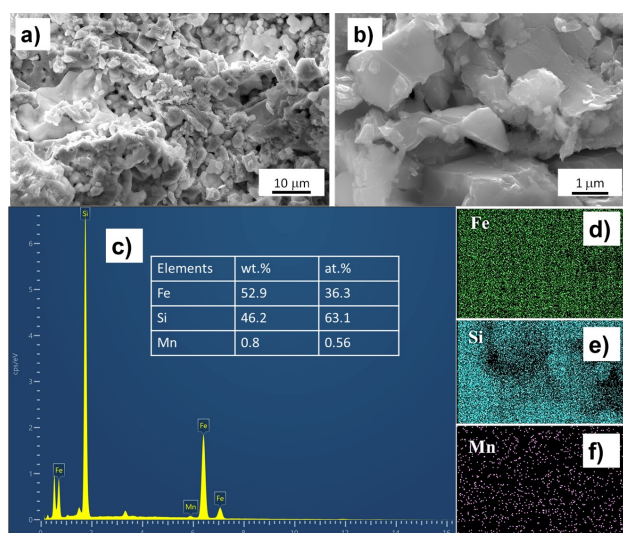


Fig. 3 Secondary Electron Micrographs of FS-1273K/15min-1073K/24h a) 10 μ m scale, b) 1 μ m scale, c) EDS spectrum, Elemental mapping d) Fe, e) Si and f) Mn.

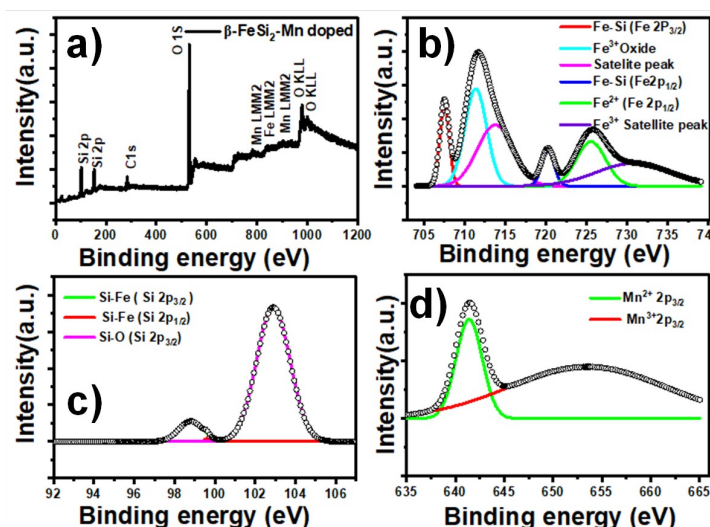


Fig. 4 X-ray Photoelectron Spectroscopy of sample FS-1273K/15min-1073K/24h a) survey spectrum b) Fe 2p spectrum, c) Si 2p spectrum and d) Mn 2p spectrum

form. The O 1s peak at 531.2 eV indicates lattice oxygen arising from Fe-O and Si-O environments due to surface oxidation. The XPS peaks corresponding to oxidized species show the thin oxide

layer formed at the surface of the material. Presence of dominant Fe-Si peak at 102-103 eV and metallic components in the surface sensitive XPS spectra suggest presence of β -FeSi₂ phase with na-



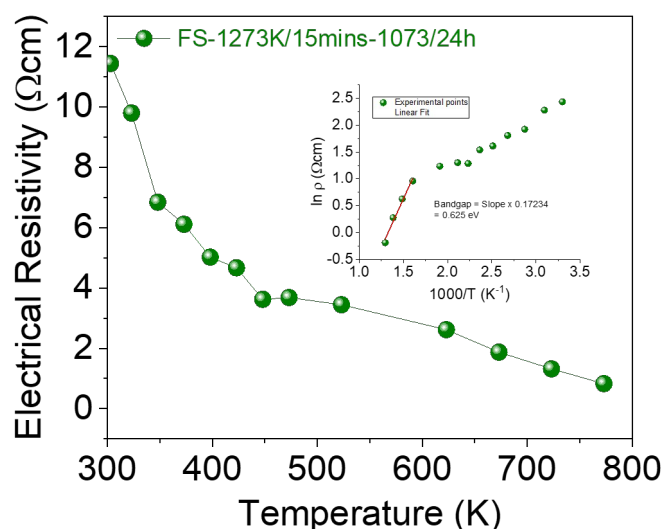


Fig. 5 Temperature-dependent electrical resistivity of sample FS-1273K/15min-1073K/24h (inset showing $1000/T$ vs $\ln \rho$)

tive oxide layer. The Mn 2p spectrum (Figure 4d) shows distinct spin-orbit splitting, with Mn $2p_{3/2}$ and Mn $2p_{1/2}$ peaks at 641.4 eV and 653.5 eV, respectively. The binding energies confirm the presence of Mn into the intermetallic or semiconducting matrix.

X-ray diffraction and X-ray photoelectron spectroscopy confirm the formation of the β -FeSi₂ phase with a minor Si secondary phase. Scanning electron microscopy and EDS analysis show a porous morphology with homogeneous elemental distribution, and the low density of the pellet (2.93 g/cm³) is also verified using Archimedes' method, further confirming the porous nature of the sample. To investigate the semiconducting behavior of the synthesized pellets, temperature-dependent resistivity measurements were performed (Figure 5). The resistivity is ~ 11 Ω .cm at room temperature and decreases to ~ 0.82 Ω .cm at 773 K. This reduction in resistivity with increasing temperature confirms the semiconducting nature of the β -FeSi₂ sample. The resistivity of the β -FeSi₂ reported in the literature typically varies between $\sim 10^{-2}$ – 1 Ω .cm, the present sample exhibits significantly higher resistivity. This is attributed to the low density and porous microstructure, which leads to poor inter-particle electrical contact, increased grain boundary scattering and minor additional contribution from the surface oxides. The measured transport properties are dominated by extrinsic microstructural effects rather than intrinsic behavior^{11,12,30}.

The temperature-dependent resistivity data were further used to plot $1000/T$ versus $\ln \rho$, from which the activation energy was estimated to be ~ 0.63 eV from the slope of the intrinsic region. The reported intrinsic band gap of β -FeSi₂ (~ 0.8 – 0.9 eV), the lower activation energy can be attributed to Mn-induced impurity states and grain boundary effects arising from the porous microstructure. Therefore, the extracted value represents an effective activation energy. The room-temperature Seebeck coefficient (S) of the as-synthesized pellet, measured using a home-built apparatus, is $+102 \pm 4$ μ V.K⁻¹ for the sample FS-1273K/15min-1073K/24h. The positive Seebeck coefficient confirms that the

sample is p-type. The power factor, calculated using $PF = S^2/\rho$, is 0.095 μ W. m⁻¹.K⁻². These values are lower than those reported in the literature for β -FeSi₂, which can be attributed to the low density of the synthesized pellets. The presence of Si secondary phase, which is a semiconductor with relatively high electrical resistivity compared to β -FeSi₂ could suppress the electrical conduction. However at this low concentration, it is expected to be present as a secondary dispersed phase rather than forming a continuous network. Therefore, its contribution is likely limited to a minor increase in overall resistivity and possible grain boundary scattering effects, without dominating the transport behavior. The temperature-dependent resistivity trend and room temperature resistivity observed suggest that bulk β -FeSi₂ conduction remains the primary transport mechanism. Although the thermoelectric properties are modest, this method is effective for synthesizing β -FeSi₂ powder, which can be useful for composite thermoelectric and photovoltaic applications.

4 Conclusions

In this work, semiconducting Mn-doped β -FeSi₂ has been successfully synthesized using the Molten salt shielded synthesis method in ambient air. The phase composition and morphology of the synthesized sample has been analyzed using XRD, SEM and EDS. The temperature dependent electrical resistivity confirms the presence of the semiconducting phase. This method provides a simple and scalable synthesis route under ambient air conditions without the need for vacuum or inert atmosphere. Overall, this study demonstrates a viable synthesis route that can be extended to large-scale synthesis of doped silicides for energy applications. Further, this method can be adopted to synthesize other oxidation prone semiconducting materials in powder form under ambient atmospheric conditions. Conventional methods rely on vacuum-assisted processes such as arc melting combined with hot pressing and prolonged heat treatment, which significantly increase manufacturing cost and limit scalability. In this work, we demonstrate a vacuum-free powder manufacturing route for silicide using simple furnace processing. Although the thermoelectric performance is limited by low density, the synthesized powders can be used for scalable composite/flexible thermoelectric and photovoltaic hybrid devices.

Author contributions

Hemalatha M Sivaprakasam: conceptualization, investigation, methodology and writing – original draft. Rajasekar Parasuraman: Conceptualization, supervision, validation and writing – review & editing. Arun Anand Prabhu: Supervision, project administration and formal analysis.

Conflicts of interest

There are no conflicts to declare.

Data availability

The data that support the findings of this study are available from the corresponding authors upon reasonable request.



Acknowledgements

The authors would like acknowledge VIT management and sponsored research office for infrastructural facilities and financial support in the form of seed grant. The authors gratefully acknowledge the Instrumentation Facility at Vellore Institute of Technology, Vellore, India, for providing the access to X-ray Diffraction (XRD), X-ray Photoelectron Spectroscopy (XPS), and Field Emission Scanning Electron Microscopy (FE-SEM) facilities.

References

- 1 X. Chen and C. Liang, *Catalysis Science & Technology*, 2019, **9**, 4785–4820.
- 2 P. Sangwan and S. Muthiah, *Journal of Materials Science: Materials in Electronics*, 2023, **34**, 1879.
- 3 J.-i. Tani and H. Kido, *Japanese Journal of Applied Physics*, 2000, **39**, 1054.
- 4 U. Birkholz and J. Schelm, *physica status solidi (b)*, 1968, **27**, 413–425.
- 5 J. Cheng, L. Gan, J. Zhang, J. Xi, L. Xi, J. Yang, T. Deng, P. Qiu, X. Shi and L. Chen, *Journal of Materials Science & Technology*, 2024, **187**, 248–257.
- 6 K. Lefki, P. Muret, N. Cherief and R. Cinti, *Journal of applied physics*, 1991, **69**, 352–357.
- 7 S. Sam, K. Yamazaki and H. Nakatsugawa, *Materials Proceedings*, 2026, **26**, 7.
- 8 K. Tan, K. Pey and D. Chi, *Journal of Applied Physics*, 2009, **106**, year.
- 9 M. Ito, H. Nagai, E. Oda, S. Katsuyama and K. Majima, *Journal of applied physics*, 2002, **91**, 2138–2142.
- 10 L. Abbassi, D. Mesguich, L. Coulomb, G. Chevallier, R. Aries, C. Estournès, E. Flahaut, R. Viennois and M. Beaudhuin, *Journal of Alloys and compounds*, 2022, **902**, 163683.
- 11 S. Sam, S. Say, K. Yamazaki and H. Nakatsugawa, *Science and Technology of Advanced Materials*, 2025, **26**, 2585555.
- 12 M. Zhu, X. Wang, Y. Yan, S. Chen, W. Zhang, H. Kang, E. Guo, Z. Chen, R. Chen and T. Wang, *ACS Applied Materials & Interfaces*, 2026.
- 13 H. Alqurashi, *International Communications in Heat and Mass Transfer*, 2026, **175**, 111244.
- 14 I. Yamauchi, S. Ueyama and I. Ohnaka, *Materials Science and Engineering: A*, 1996, **208**, 108–115.
- 15 P. E. Turchi, V. I. Ivashchenko, V. Shevchenko, L. Gorb, J. Leszczynski and A. Perron, *Applied Sciences*, 2023, **13**, 12669.
- 16 I. Yamauchi, T. Okamoto, H. Ohata and I. Ohnaka, *Journal of alloys and compounds*, 1997, **260**, 162–171.
- 17 K. Han, M. Saito, J. Xia, I. Ohnuma and R. Kainuma, *Journal of Alloys and Compounds*, 2022, **919**, 165810.
- 18 U. Ail, S. Gorsse, S. Perumal, M. Prakasam, A. Umarji, S. Vivès, P. Bellanger and R. Decourt, *Journal of Materials Science*, 2015, **50**, 6713–6718.
- 19 P. Rajasekar and A. M. Umarji, *Intermetallics*, 2017, **89**, 57–64.
- 20 F. L. B. M. Redzuan, I. Mikio and T. Masatoshi, *Journal of Materials Science*, 2018, **53**, 7683–7690.
- 21 S.-C. Ur, I.-H. Kim and J.-I. Lee, *Metals and Materials International*, 2002, **8**, 169–175.
- 22 T. Yamada and H. Yamane, *Chemistry of Materials*, 2007, **19**, 6047–6051.
- 23 T. Yamada, H. Morito and H. Yamane, *Japanese Journal of Applied Physics*, 2009, **48**, 100209.
- 24 L. Abbassi, D. Mesguich, L. Coulomb, G. Chevallier, R. Aries, C. Estournès, E. Flahaut, R. Viennois and M. Beaudhuin, *Journal of Alloys and compounds*, 2022, **902**, 163683.
- 25 W. Shen, S. Shen, W. Tang and L. Wang, *Narrow Gap Semiconductors 1995*, CRC Press, 2020, pp. 90–94.
- 26 K. Lefki, P. Muret, N. Cherief and R. Cinti, *Journal of applied physics*, 1991, **69**, 352–357.
- 27 S. Muthiah *et al.*, *Ceramics International*, 2022, **48**, 29366–29371.
- 28 P. Sangwan, N. K. Upadhyay, R. Shyam, P. Gupta, H. Kumar, S. Singh, A. Pandey and S. Muthiah, *Hybrid Advances*, 2025, **9**, 100423.
- 29 A. Dash, R. Vaßen, O. Guillon and J. Gonzalez-Julian, *Nature materials*, 2019, **18**, 465–470.
- 30 F. Esaka, H. Yamamoto, H. Udono, N. Matsubayashi, K. Yamaguchi, S. Shamoto, M. Magara and T. Kimura, *Applied Surface Science*, 2011, **257**, 2950–2954.
- 31 S. Sen, P. Guha, P. Banerji and P. Pramanik, *RSC advances*, 2016, **6**, 68238–68246.





VIT[®]
Vellore Institute of Technology
(Deemed to be University under section 3 of UGC Act, 1956)

View Article Online
DOI: 10.1039/D6MA00411C

Dr. Rajasekar P.

Assistant Professor
Department of Chemistry
School of Advanced Sciences
Vellore Institute of Technology
Vellore, Tamil Nadu, India -632 014

Phone: +91-9611157741
E-mail: rajasekar.mgac@gmail.com

Dear Editor

We are pleased to submit our manuscript entitled “Low-temperature Molten Salt Shielded Synthesis of Semiconducting β -FeSi₂ in ambient air condition” by Hemalatha M. Sivaprakasam to Journal of Materials Chemistry A.

On behalf of all the authors I confirm that “The data that support the findings of this study are available from the corresponding authors upon reasonable request.”

Yours sincerely

(Rajasekar P.)

